Semiconductor Science and Technology

PAPER • OPEN ACCESS

Correlations between reverse bias leakage current, cathodoluminescence intensity and carbon vacancy observed in 4H-SiC junction barrier Schottky diode

To cite this article: Lok-Ping Ho *et al* 2023 *Semicond. Sci. Technol.* **38** 115007

View the article online for updates and enhancements.

You may also like

- Spatio-time-resolved cathodoluminescence studies of wide-bandgap group-III nitride semiconductors
Shigefusa F. Chichibu, Yoichi Ishikawa, Kouji Hazu et al.

- Electron beam dose dependence of surface recombination velocity and surface space charge in semiconductor nanowires
Fabrice Donatini, Corinne Sartel, Vincent Sallet et al.

- Quenching of the luminescence intensity of GaN nanowires under electron beam exposure: impact of C adsorption on the exciton lifetime
Jonas Lähnemann, Timur Flissikowski, Martin Wölz et al.

ECS The Electrochemical Society
Advancing solid state & electrochemical science & technology

ECS UNITED

247th ECS Meeting
Montréal, Canada
May 18-22, 2025
Palais des Congrès de Montréal

Showcase your science!

Abstracts due December 6th

This content was downloaded from IP address 175.159.182.11 on 23/09/2024 at 02:33

OPEN ACCESS
IOP Publishing

Semiconductor Science and Technology

Semicond. Sci. Technol. **38** (2023) 115007 (5pp)

https://doi.org/10.1088/1361-6641/acfb32

Correlations between reverse bias leakage current, cathodoluminescence intensity and carbon vacancy observed in 4H-SiC junction barrier Schottky diode

Lok-Ping Ho[1,2], Si-hua Li[1], Tianxiang Lin[1], Jack Cheung[2], Tony Chau[2] and Francis Chi-Chung Ling[1,*]

[1] Department of Physics, The University of Hong Kong, Pokfulam Road, Hong Kong Special Administrative Region of China, People's Republic of China
[2] Alpha Power Solutions Ltd, Hong Kong Special Administrative Region of China, People's Republic of China

E-mail: ccling@hku.hk

Received 31 May 2023, revised 25 August 2023
Accepted for publication 18 September 2023
Published 10 October 2023

Abstract

Reverse bias currents of ten commercial junction barrier Schottky diodes were measured, and the dies were studied by scanning electron microscope (SEM) and cathodoluminescence (CL) after the de-capsulation of the diodes. Defect emissions (DEs) of 2.62 eV were observed in all the CL spectra. By comparing the SEM images, the integral CL intensity spatial mappings and the reverse bias leakage currents, correlations between the leakage current, the integral CL intensity and the Al-implantation process were established. The data of reverse bias leakage current against the reverse bias voltage taken at room temperature followed the Poole Frenkel emission from the Z_1/Z_2 carbon vacancy states to the conduction band. The DE at 2.62 eV is associated with the electronic transition from Z_1/Z_2 to the valence band. The current observation also opens up the feasibility of screening off SiC diodes with large leakage current during production by inspecting the CL intensity before the device fabrication is complete.

Supplementary material for this article is available online

Keywords: cathodoluminescence, leakage current, defect

(Some figures may appear in colour only in the online journal)

[*] Author to whom any correspondence should be addressed.

Original content from this work may be used under the terms of the Creative Commons Attribution 4.0 licence. Any further distribution of this work must maintain attribution to the author(s) and the title of the work, journal citation and DOI.

© 2023 The Author(s). Published by IOP Publishing Ltd

1. Introduction

Compared to silicon, 4H-SiC has a larger bandgap (3.25 eV), higher breakdown electric field (2.5 $\mathrm{MCcm^{-1}}$), higher saturated carrier velocity (2×10^7 $\mathrm{cm^{-1}}$) and better thermal conductivity (4.9 $\mathrm{Wcm^{-1}K^{-1}}$). These supreme physical properties make SiC a better choice for fabricating high-power devices. Atomic-scale intrinsic defects in semiconductors have deep ionization states in the band gap and a significant influence on the electrical properties of the materials and the corresponding devices. Carbon vacancy is the dominant intrinsic defect in 4H-SiC, having ionization states at 0.6–0.7 eV and 1.5–1.6 eV below the conduction band (denoted by $Z_{1/2}$ and $EH_{6/7}$, respectively) [1–6]. Carbon vacancy has a typical concentration of 10^{12} $\mathrm{cm^{-3}}$ in as-grown 4H-SiC epi, and goes up to 10^{15} $\mathrm{cm^{-3}}$ after annealing at 1950 °C [3]. V_C is reported to have the effect of decreasing the carrier lifetime in SiC devices [7–9], influencing the forward current-voltage characteristics of 4H-SiC p–i–n diodes [10] and increasing the reverse bias leakage current [11]. Al-ion implantation followed by high-temperature annealing is crucial to introduce p-type doping in 4H-SiC bipolar device fabrication [5]. Carbon vacancy was created in the ion-implantation and subsequent high temperature annealing [12]. It is thus important to have a probe capable of characterizing carbon vacancy in the line of the SiC device fabrication.

There are many methods for detecting electronic defect states in the band gap in semiconductor materials and devices, such as deep level transient spectroscopy (DLTS) [1, 3, 4, 6, 9, 13] and luminescence spectroscopy [13–15]. DLTS can reveal the deep trap activation energy and concentration by monitoring the capacitance transient during the reverse bias pulse period after the forward bias trap filling pulse is applied. Luminescence spectroscopy can be used to detect deep trap states by observing the defect emission (DE) resulting from the electronic transition between states, for example, the conduction band to defect state transition or the defect state to valence band transition. Carrier excitation is needed for luminescence spectroscopy, whereas a laser with photon energy larger than the band gap is used in photoluminescence and accelerating electrons are used in cathodoluminescence (CL). Fabbri *et al* [13] compared the spectra of CL and DLTS of Al-ion implanted 4H-SiC diodes, reporting a correlation between a broad DE centered at 2.5 eV and the DLTS signal Z_1/Z_2 (with activation energy of 0.66 eV). Scanning electron microscopes (SEM) are probes which can revealdefects on a surface via morphological imaging. Defect review SEM is a useful tool capable of being installed in the device production line to reveal the surficial defect image on the wafer [16]. It is not easy to detect atomic scale defects such as vacancy by SEM imaging, however, for *in-situ* detection of deep traps during the manufacturing process, DLTS may not be easily encorporated into the production line, as the method needs to be performed on the rectifying diode.

2. Experimental

The samples are commercial JBS diodes with the detailed fabrication processes given as for the Batch A samples in [17]. The 4H-SiC epi has an electron concentration of 10^{16} $\mathrm{cm^{-3}}$. Multi-step Al-implantation was performed in a square ring-shaped region to create a $\sim$1 μm depth box-shaped doping of $p \sim 10^{20}$ Al $\mathrm{cm^{-3}}$. Thermal annealing at 1950 °C in Ar was then carried out to activate the Al doping. Ti deposition is then performed on the front and back sides for the metal contacts and then capsulated.

The reverse bias leakage current of the samples was measured and monitored at room temperature with a bias of -1700 V. Ten representative samples with leakage current lying in a wide range from $\sim$1 μA to 100 μA were chosen. The ten samples were de-capsulated by wet chemical etching. The samples were etched by being immersed in H_2SO_4/H_2O_2 for 10 min and HF for 10 min. After removing the surface electrode, the samples were rinsed with deionized water. The size of each die is $\sim$0.3 mm $\times$ 0.3 mm. SEM characterization was carried out using the JEOL field emission SEM JSM-7001-F and the CL study was performed using the attached monochromator GATAN MonoCL3. For each die, SEM and CL studies were conducted at nine different sampling positions of the die after de-capsulation. While carrying out the CL measurements, the power was kept constant at 30 μW and electron acceleration voltage of 10 kV so that the comparison of CL intensity between samples was feasible.

3. Result

Table 1 tabulates the reverse bias leakage currents of the ten diodes while biased at -1700 V. The leakage current I_{leakage} varied from 0.86 μA to 139 μA. Sample 10 is the sample with the largest I_{leakage} (=139 μA). The SEM images taken at the nine different locations are given in figure S1(a) in the supplementary information figure S1, whereas a typical one is shown in figure 1(a). The nine locations of the CL measurements sampled over the whole area of sample 10 (see figure S1(b)). CL measurements were also conducted in the regions of the SEM images. The spatial mappings of the CL intensity summing over the photon energy of 1.75–4.13 eV taken at the corresponding nine different positions are shown in figure S1(b) in the SI. The CL intensity spatial mapping associated with the SEM image in figure 1(a) is given in figure 1(b). The red dotted square labels one of the regions with Al-ion implantation. The SEM images and the corresponding CL intensity spatial mappings of sample 6 (which has a lower $I_{\mathrm{leakage}} = 12.6$ μA) sampled at the nine different positions are shown in figure S2 of the SI. Figures 1(c) and (d) show one of the typical SEM images and the corresponding CL intensity spatial mapping for sample 6. The SEM images and the corresponding CL intensity spatial mappings taken at the nine different positions of

Table 1. The reverse bias leakage current of ten diodes at −1700 V.

Diode number	1	2	3	4	5	6	7	8	9	10
$I_{leakage}$ (μA)	0.86	1.40	1.42	1.43	2.21	12.6	13.5	20.1	37.0	139

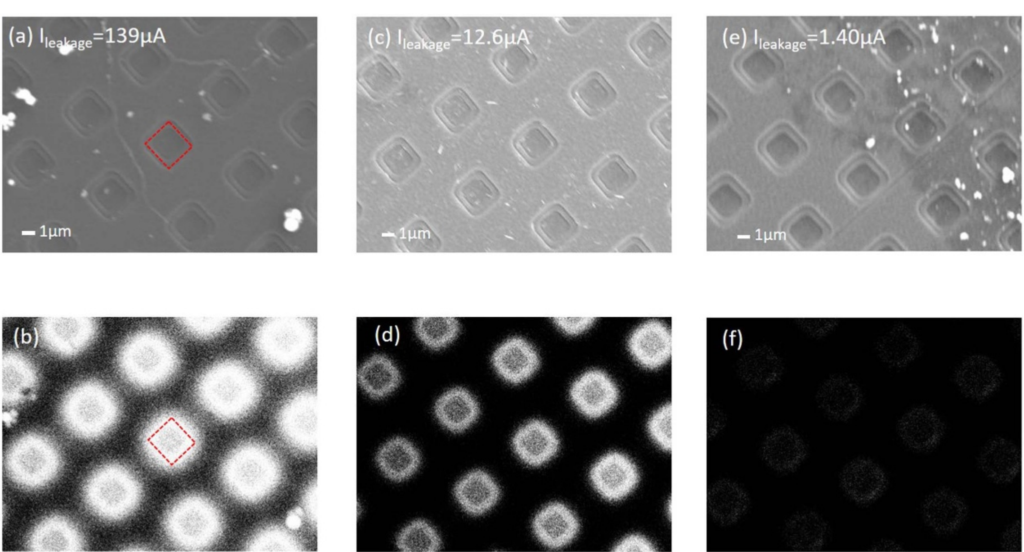

Figure 1. Shows the SEM images and the corresponding CL intensity spatial mappings of sample 10 ((a) and (b)); sample 6 ((c) and (d)); and sample 2 ((e) and (f)). The red dotted lines indicate one of the Al-ion implantation regions.

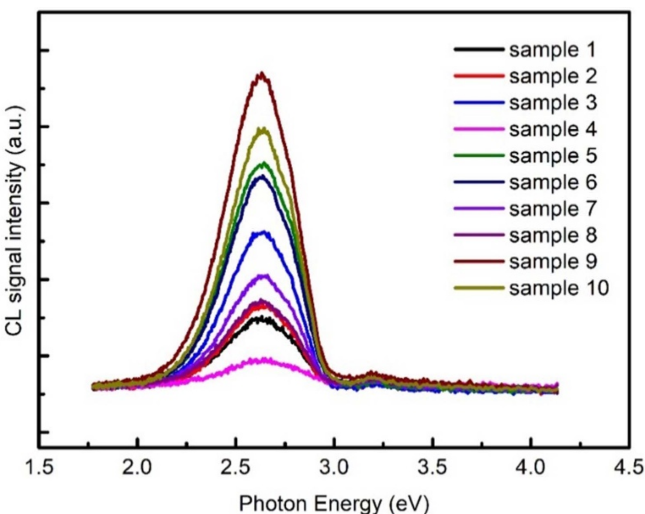

Figure 2. Shows the CL spectra of the different samples. The CL signal intensity of a particular photon energy shown is obtained by summing the CL intensity over the whole area of the corresponding SEM images taken at nine different locations of the sample.

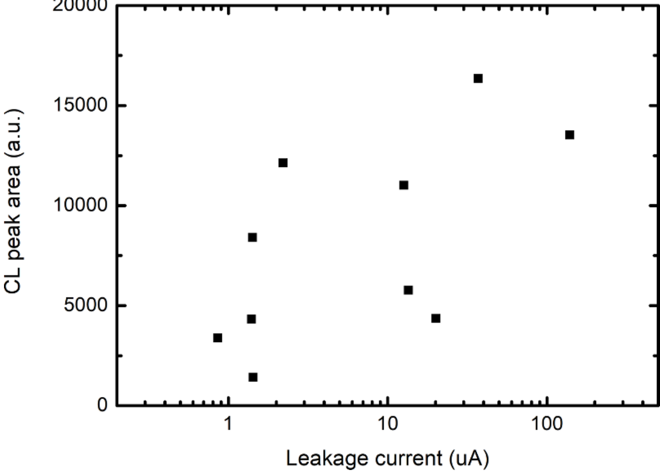

Figure 3. Shows the integral CL intensities against the reverse bias leakage currents for each of the samples. The reverse bias applied is −1200 V. The integral CL intensity corresponds to the area of the 2.62 eV CL peak shown in the CL spectrum (figure 2).

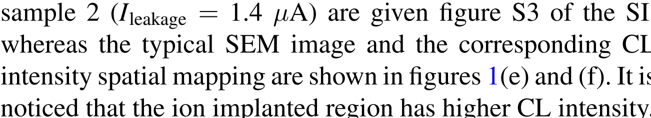

sample 2 ($I_{leakage}$ = 1.4 μA) are given figure S3 of the SI, whereas the typical SEM image and the corresponding CL intensity spatial mapping are shown in figures 1(e) and (f). It is noticed that the ion implanted region has higher CL intensity.

Figure 2 shows the CL spectra (i.e. luminescence intensity versus photon energy) for all the samples in the photon energy range of 1.75–4.13 eV, with the intensities obtained by summing over the whole SEM image region. A peak is observed at a photon energy of 2.62 eV in all of the CL spectra. For each sample, the integral CL intensity I_{CL} in the energy range of 1.75–4.13 eV is calculated by summing over the intensity of the CL spectra in the energy range. The thus obtained log of the integral CL intensity is plotted against the log of the reverse bias leakage current in figure 3. Although the physical model and equation describing the relation between the integral CL intensity and the leakage current is not yet known and requires further study, a positive correlation is noticed between $\log(I_{CL})$ and $\log(I_{leakage})$. The data of $\log(I_{CL})$ vs $\log(I_{leakage})$

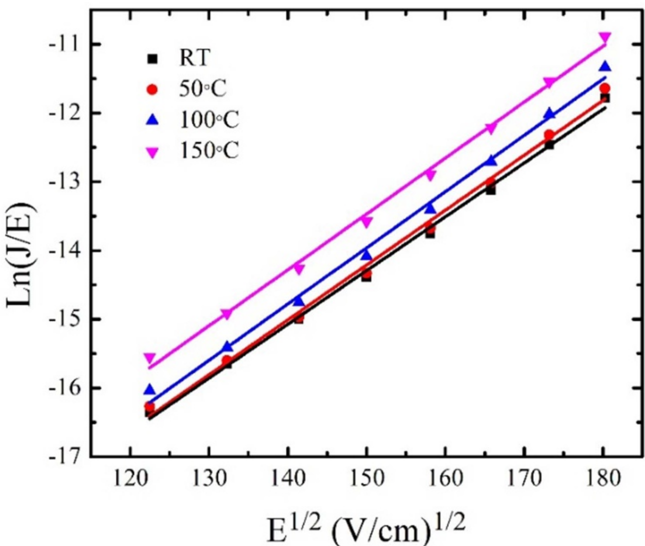

Figure 4. Shows the Ln(J/E) against $E^{1/2}$ of Sample 6 taken at different temperatures from room temperature to 150 °C. The straight lines refer to the fitted lines with equation (1).

looks scattered. It can be understood in terms of the sample preparation process for the CL measurement involving acid etching to remove the encapsulation, which would not be able to be precisely controlled upon each of the individual samples.

To further understand the reverse bias current, we studied the reverse bias current against the applied reverse bias (−75 V to −1200 V) at different temperatures (room temperature to 150 °C) on a new commercial JBS diode fabricated by the same process (sample 11). Figure 4 shows the corresponding Ln(J/E) against $E^{1/2}$. E is the electric field of the corresponding electric bias. The Poole–Frenkel (PF) emission current involves carrier emission from a defect to the conduction band, and is given by [18, 19]:

$$J = KE\ \exp\left\{-q\left(\Phi_{\mathrm{T}} - \sqrt{qE/\pi\varepsilon_{\mathrm{s}}\varepsilon_0}\right)/kT\right\} \quad (1)$$

where K is a constant depending on the carrier concentration and Φ_{T} is the ionization energy of the trap. The linear relation between Ln (J/E) against $E^{1/2}$ implies that the PF emission current is the dominant process for the reverse bias leakage current. The ionization energies of the traps are fitted using equation (1) on the data and the results are tabulated in table 2. The ionization energy obtained at the RT is 0.65 eV, which coincides well with the E_{a} of the carbon vacancy (Z_1/Z_2) observed in the DLTS measurement [3, 4, 6, 9, 13]. This implies that the reverse biased leakage current is dominated by the PF emission from the carbon vacancy Z_1/Z_2 states to the conduction band.

It is noticed that the ionization energy obtained from the fitting increases with temperature to value of 0.92 eV at 150 °C. The leakage current may originate from traps other than the carbon vacancy states due to PF emission. One possible candidate is the trap having ionization energy $\Phi_{\mathrm{T}} = 1.03$ eV, which is associated with a carbon cluster [20]. Higher temperatures enhance the thermal excitation, and thus PF emission from deeper states like carbon clusters emerges, becoming more effective and feasible. The fitted ionization energy is indeed the corresponding effective ionization energy. The observed increase of the fitted effective ionization energy with temperature indicates emission from deeper states at higher temperatures.

Table 2. PF emission fitting results in different temperature.

Temperature (°C)	RT	50	100	150
Ionization energy (eV)	0.65	0.69	0.82	0.92

4. Discussion

The results presented above provide evidence that the reverse bias current at room temperature of the device is dominated by the PF emission from the carbon vacancy Z_1/Z_2 states to the conduction band. It is also worth discussing the origin of the 2.62 eV emission peak in the CL spectrum. Comparing the SEM images with the corresponding CL intensity spatial mappings in figures 1, S1 and S2, the CL is associated with the Al implantation. A similar observation in the correlation between CL (∼2.5 eV) and the Al implantation was observed by Fabbri *et al* [13]. Furthermore, Fabbri *et al* [13] observed the correlation between the CL intensity and the DLTS signal of Z_1/Z_2. The band gap of 4H-SiC is 3.26 eV at room temperature. Carbon vacancies have trap states Z_1/Z_2 at 0.6–0.7 eV below the conduction band E_{C}. The energy difference between the Z_1/Z_2 and the valance band is thus ∼2.5–2.6 eV, and thus the 2.62 eV DE observed in the current study could be attributed to the electronic transition from Z_1/Z_2 to valance band transition. Chen *et al* [21] reported introduction of DEs (2.56 eV and 2.81 eV) in the CL spectra of 4H-SiC after the Cu implantation. The 2.56 eV DE was associated with Z_1/Z_2.

The correlation between the reverse bias leakage current and the integral CL emission intensity observed in the current study can now be explained. Both the reverse bias leakage current and the integral CL emission intensity are associated with the carbon vacancy through the PF emission and electronic transition from the conduction band to the carbon vacancy state. Thus, the higher concentration of V_{C} leads to larger reverse bias leakage current and integral CL emission intensity.

Atomic scale defects in materials have a significant influence on the device performance. For example, V_{C} is commonly found in 4H-SiC epi materials. It can be thermally generated during the high temperature fabrication process, such as the annealing activation of the Al p-type dopant after the Al-ion implantation [12]. The presence of V_{C} would degrade the device performance, such as decreasing the minority carrier

lifetime [7–9] and increasing the reverse bias leakage current of the JBS diode [11]. However, characterizing atomic scale defects during in-line device manufacturing is not trivial. DLTS is a commonly used method to characterize deep traps in semiconductors including 4H-SiC [4, 22]. This method involves the filling of deep traps while the diodes are in forward or zero, followed by the measurement of the capacitance transient in the depletion region while the diode is put under reverse bias. Characterizing defects by DLTS requires the rectifying diode and thus is not easy during the on-line device fabrication process before the device is completed. SEMs are now adopted by all advanced wafer fabrication lines for imaging and reviewing sub-micron defects [23]. With advanced classification schemes, yield limiting defects (killers) are separated from non-yield limiting defects (non-killers). However, SEMs can only detect sub-micron size defects but are not able to detect electrical active atomic-scale defects which would significantly influence the device performance. There is currently no available methodology used in fabrication sites during the on-line fabrication to detect atomic scale defects which significantly influence the performance of the resultant devices. The present study reveals the correlation between the 4H-SiC diode leakage current and the integral CL intensity, while the reverse bias leakage current and the integral CL intensity of the 2.62 eV peak are associated with the carbon vacancy via the PF emission and electronic transition involving the carbon vacancy. Carbon vacancies are introduced in many energetic processes and thermal processes during SiC device fabrication, such as Al-ion implantation and high temperature annealing. The current results open up the feasibility of employing CL as a probe in the manufacturing line to detect carbon vacancies and screen off the devices in production that would yield large reverse bias leakage currents. Through the spatial mapping of the integral CL intensity, the spatial distribution of the carbon vacancy can also be obtained. Moreover, CL can be installed in the SEM used to carry out defect inspection during the fabrication process.

5. Conclusion

In summary, correlations between the reverse bias current, CL intensity and carbon vacancy were observed, whereas the CL originates from the electronic transition from the conduction band to the carbon vacancy Z_1/Z_2 states and the leakage current is dominated by the PF emission from the carbon vacancy Z_1/Z_2 states to the conduction band. This also opens the feasibility of screening off the devices with large reversed bias current during the production line using on-line CL inspection before the device fabrication processes complete.

Data availability statement

All data that support the findings of this study are included within the article (and any supplementary files).

Acknowledgments

This work is supported by the Key-Area Research and Development Program of Guangdong Province (No. 2020B010170002) and the Innovation and Technology Fund, HKSAR (No. ITS/215/20FP).

ORCID iDs

Tianxiang Lin https://orcid.org/0000-0002-5095-7746
Francis Chi-Chung Ling https://orcid.org/0000-0003-4757-1065

References

[1] Negoro Y, Kimoto T and Matsunami H 2004 *Appl. Phys. Lett.* **85** 1716
[2] Yan X, Li P, Kang L, Wei S-H and Huang B 2020 *J. Appl. Phys.* **127** 085702
[3] Ayedh H M, Bobal V, Nipoti R, Hallén A and Svensson B G 2014 *J. Appl. Phys.* **115** 012005
[4] Hemmingsson C, Son N T, Kordina O, Bergman J P, Janzén E, Lindström J L, Savage S and Nordell N 1997 *J. Appl. Phys.* **81** 6155
[5] Nipoti R, Ayedh H M and Svensson B G 2018 *Mater. Sci. Semicond. Process.* **78** 13
[6] Storasta L, Tsuchida H, Miyazawa T and Ohshima T 2008 *J. Appl. Phys.* **103** 013705
[7] Klein P B, Shanabrook B V, Huh S W, Polyakov A Y, Skowronski M, Sumakeris J J and O'Loughlin M J 2006 *Appl. Phys. Lett.* **88** 052110
[8] Storasta L and Tsuchida H 2007 *Appl. Phys. Lett.* **90** 062116
[9] Hiyoshi T and Kimoto T 2009 *Appl. Phys. Express* **2** 041101
[10] Megherbi M L, Pezzimenti F, Dehimi L, Saadoune M A and Della Corte F G 2018 *IEEE Trans. Electron Devices* **65** 3371
[11] Zhao L, Tang Y, Bai Y, Qiu M, Wu Z, Yang Y, Yang C, Tian X and Liu X 2022 *Electronics* **11** 1341
[12] Ayedh H M, Kvamsdal K E, Bobal V, Hallén A, Ling F C C and Kuznetsov A Y 2021 *J. Appl. Phys.* **54** 455106
[13] Fabbri F, Natalini D, Cavallini A, Sekiguchi T, Nipoti R and Moscatelli F 2009 *Superlattices Microstruct.* **45** 383
[14] Maximenko S I, Freitas J A Jr, Klein P B, Shrivastava A and Sudarshan T S 2009 *Appl. Phys. Lett.* **94** 092101
[15] Ling C C, Chen X D, Gong M, Yang C L, Ge W K and Wang J N 2006 *Phys. Rev.* B **376** 374
[16] Jain A, Sheridan J G, Xing R, Levitov F, Yasharzade S and Nguyen H 2017 *2017 28th Annual SEMI Advanced Semiconductor Manufacturing Conf. (ASMC)* (*Saratoga Springs, USA*, *2017*) pp 240–8
[17] Lin T, Li S-H, Ho L-P, Kuznetsov A, Lee H N, Chau T and Ling F C-C 2023 *IEEE Electron Device Lett.* **44** 578
[18] Yeargan J R and Taylor H L 1968 *J. Appl. Phys.* **39** 5600
[19] Yıldız D E, Karadeniz S and Gullu H H 2021 *J. Mater. Sci., Mater. Electron.* **32** 20130
[20] Alfieri G and Kimoto T 2012 *J. Appl. Phys.* **112** 6
[21] Chen B, Matsuhata H, Sekiguchi T, Ohyanagi T, Kinoshita A and Okumura H 2010 *Appl. Phys. Lett.* **96** 212110
[22] Capan I, Brodar T, Bernat R, Pastuović Ž, Makino T, Ohshima T, Gouveia J D and Coutinho J 2021 *J. Appl. Phys.* **130** 125703
[23] Abraham Z 2001 *Proc. SPIE* **4275** 99